BIOCHEMISTRY
including biophysical chemistry & molecular biology

Article

pubs.acs.org/biochemistry

Structure of a Sugar *N*-Formyltransferase from *Campylobacter jejuni*[¶]

James B. Thoden,[†] Marie-France Goneau,[‡] Michel Gilbert,[‡] and Hazel M. Holden*[,†]

[†]Department of Biochemistry, University of Wisconsin, Madison, Wisconsin 53706, United States

[‡]Human Health Therapeutics, National Research Council Canada, Ottawa, Ontario K1A OR6, Canada

ABSTRACT: The O-antigens, which are components of the outer membranes of Gram-negative bacteria, are responsible for the wide species variations seen in nature and are thought to play a role in bacterial virulence. They often contain unusual dideoxysugars such as 3,6-dideoxy-3-formamido-D-glucose (Qui3NFo). Here, we describe a structural and functional investigation of the protein C8J_1081 from *Campylobacter jejuni* 81116, which is involved in the biosynthesis of Qui3NFo. Specifically, the enzyme, hereafter referred to as WlaRD, catalyzes the *N*-formylation of dTDP-3,6-dideoxy-3-amino-D-glucose (dTDP-Qui3N) using N^{10}-formyltetrahydrofolate as the carbon source. For this investigation, seven X-ray structures of WlaRD, in complexes with various dTDP-linked sugars and cofactors, were determined to resolutions of 1.9 Å or better. One of the models, with bound N^{10}-formyltetrahydrofolate and dTDP, represents the first glimpse of an *N*-formyltransferase with its natural cofactor. Another model contains the reaction products, tetrahydrofolate and dTDP-Qui3NFo. In combination, the structures provide snapshots of the WlaRD active site before and after catalysis. On the basis of these structures, three amino acid residues were targeted for study: Asn 94, His 96, and Asp 132. Mutations of any of these residues resulted in a complete loss of enzymatic activity. Given the position of His 96 in the active site, it can be postulated that it functions as the active site base to remove a proton from the sugar amino group as it attacks the carbonyl carbon of the *N*-10 formyl group of the cofactor. Enzyme assays demonstrate that WlaRD is also capable of utilizing dTDP-3,6-dideoxy-3-amino-D-galactose (dTDP-Fuc3N) as a substrate, albeit at a much reduced catalytic efficiency.

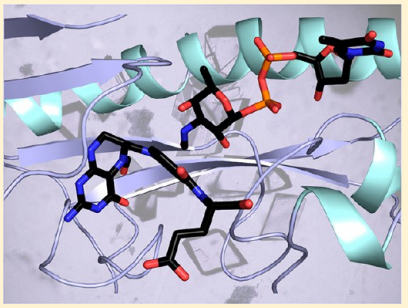

The outer membranes of Gram-negative bacteria are characterized by a complex lipoglycan referred to as the lipopolysaccharide, or LPS. It can be envisioned in terms of three components: (1) lipid A, which serves to anchor the LPS to the outer membrane, (2) the core oligosaccharide, which contains sugars such as glucose, galactose, and *N*-acetylglucosamine as well as some seven-carbon sugars, and (3) the O-antigen or O-polysaccharide, which extends farthest away from the bacterium. Several mucosal pathogens, such as *Neisseria*, *Haemophilus*, and *Campylobacter* spp., lack O-polysaccharide repeating units and display considerable structural diversity in their outer core glyans.[1] These low molecular weight LPS variants are referred to as lipooligosaccharides (LOS).

The O-polysaccharides and LOS outer cores often contain unusual sugars such as colitose, paratose, or tyvelose, among others.[2] Indeed, more than 100 different di-, tri-, and tetradeoxysugars have been isolated from prokaryotic sources thus far.[3] Whereas it has been established that lipid A is a major contributor to the toxicity of Gram-negative bacterial infections, the biological role of the O-polysaccharide is less well understood. Recent studies suggest that it is important for the effective colonization of host tissues and for resistance to complement-mediated killing.[4]

Through the efforts of numerous laboratories, a better understanding of the manner in which unusual di-, tri-, and tetradeoxysugars are biochemically synthesized has been obtained.[5] Many are constructed around the nucleotide-linked 3,6-dideoxyhexoses, which are further modified by acetylation, amination, epimerization, and *C*-, *N*-, and *O*-methylation reactions. At present, there is a substantial body of literature describing these types of enzymatic modifications. There is still a paucity of structural and kinetic data on *N*-formyltransferases, however, that function specifically on nucleotide-linked sugars. This is somewhat surprising given that the existence of *N*-formylated sugars was reported back in 1985.[6] Thus far, only two biochemical studies have been described on sugar *N*-formyltransferases. The first was on ArnA from *Escherichia coli*, which catalyzes the conversion of UDP-4-amino-4-deoxy-L-arabinose to UDP-4-formamido-4-deoxy-L-arabinose.[7] ArnA is a bifunctional protein, with the N-terminal domain functioning as the *N*-formyltransferase and the C-terminal domain catalyzing an oxidative decarboxylation reaction. The second enzyme investigated, VioF from *Providencia alcalifaciens* O3, catalyzes the conversion of dTDP-4-amino-4,6-dideoxy-D-glucose to dTDP-4-formamido-4,6-dideoxy-D-glucose.[8] Both ArnA and VioF use N^{10}-formyltetrahydrofolate (N^{10}-formyl-THF) as the formyl donor. A crystal structure of the N-terminal domain of ArnA was determined in the presence of N^5-formyltetrahydrofolate (N^5-formyl-THF) and UMP, but details concerning the active site architecture were limited due to the absence of a bound nucleotide-linked sugar.[9]

Campylobacter jejuni 81116 (Penner serotype HS:6) has a class E LOS biosynthesis locus containing 19 genes. This locus includes 11 homologues of glycosyltransferases, one lipid A

Received: July 8, 2013
Revised: July 30, 2013
Published: July 30, 2013

   dx.doi.org/10.1021/bi4009006 | *Biochemistry* 2013, 52, 6114−6126

acyltransferase, and 7 genes involved in either the biosynthesis of dideoxyhexosamine residues (ddHexN) or in their modifications.[10] The basic composition of the *C. jejuni* LOS outer core has been proposed through mass spectrometry analysis, and it has been suggested that it contains two ddHexN residues that can be either acetylated or formylated.[10] However, the complexity and heterogeneity of the glycans produced by *C. jejuni* 81116 prevented the complete structural determination of the LOS outer core by NMR. In addition, two other polysaccharides are produced by *C. jejuni* 81116: polysaccharide A, which contains glucose, glucuronic acid, and mannose, and polysaccharide B, which contains glucose, galactose, and *N*-acetylglucosamine.[11]

Recently, we have shown that the hypothetical protein C8J_1081 from *C. jejuni* 81116 catalyzes the transfer of a formyl group to either dTDP-3-amino-3,6-dideoxy-D-glucose (dTDP-Qui3N) or dTDP-3-amino-3,6-dideoxy-D-galactose (dTDP-Fuc3N) as indicated in Scheme 1 (the protonation states

Scheme 1

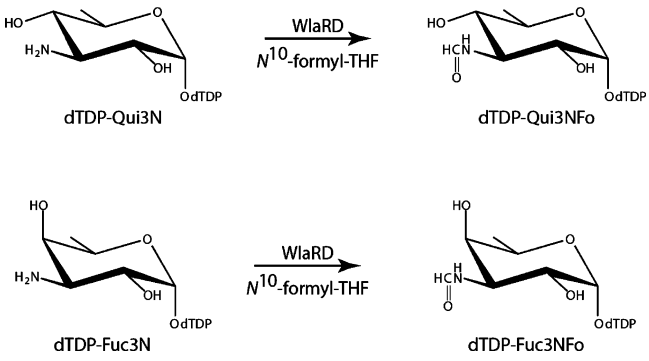

of these substrates, when bound in the enzyme's active site, are not known). Here we report a combined structural and functional investigation of this enzyme, hereafter referred to as WlaRD. For this analysis, seven structures were determined to a resolution of 1.9 Å or better: complexes of the enzyme with N^5-formyl-THF and dTDP, dTDP-Qui3N, dTDP-Fuc3N, or dTDP-3,6-dideoxy-3-formamido-D-galactose (dTDP-Fuc3NFo), complexes of the enzyme with N^{10}-formyl-THF and dTDP or dTDP-glucose, and a complex of WlaRD with tetrahydrofolate (THF) and dTDP-3,6-dideoxy-3-formamido-D-glucose (dTDP-Qui3NFo). On the basis of these structures, site-directed mutant proteins were constructed and their kinetic parameters measured. Taken together, these studies provide, for the first time, a glimpse of a fully loaded sugar *N*-formyltransferase active site and reveal how enzymes in this class bind N^{10}-formyl-THF.

MATERIALS AND METHODS

Cloning of *wlaRD*. The following primers were designed to amplify ORF C8J_1081 (or WlaRD, GeneBank Accession number ABV52680) from *C. jejuni* 81116: CJ-1030, 5′-ACGAGTTCTGC*ATATG*ATTAAAATATGTATAGCTGGAAAAAAC-3′ (43-mer, NdeI site in italics); CJ-1032, 5′-CGGTAG*TCGAC*TTAGTGATGGTGATGGTGATGTAACTTATTTAATTTTTGAGCG-3′ (54-mer, SalI site in italics, 6-His tag underlined). The Phusion high fidelity DNA polymerase (New England Biolabs, Beverly, MA) and 100 ng of genomic DNA were used to obtain a PCR product that was digested with NdeI and SalI and initially cloned into pCWori+(*-lacZ*), giving plasmid CJV-19.

A version encoding WlaRD with a TEV-cleavable N-terminal His tag was subsequently created by utilizing CJV-19 as a PCR template. The primers used incorporated NdeI, 5′-*CATATG*-ATTAAAATATGTATAGCTGGAAAAAACAATATTGCC-3′, and XhoI, 5′-*CTCGAG*TAACTTATTTAATTTTTGA-GCGATAATTTTAAATCC-3′, restriction sites. Platinum Pfx DNA polymerase (Invitrogen) was used for amplification. The PCR product was digested with NdeI and XhoI and ligated into pET28t, a lab pET28b(+) vector that had been previously modified to incorporate a TEV protease recognition site after the N-terminal polyhistidine tag.[12]

Protein Expression and Purification. The pET28t-WlaRD plasmid was used to transform Rosetta2(DE3) *E. coli* cells (Novagen). The cultures were grown in lysogeny broth supplemented with kanamycin and chloramphenicol at 37 °C with shaking until an optical density of 0.8 was reached at 600 nm. The flasks were cooled in an ice bath, and the cells were induced with 1 mM IPTG and allowed to express protein at 16 °C for 24 h.

The cells were harvested by centrifugation and disrupted by sonication on ice. The lysate was cleared by centrifugation, and WlaRD was purified utilizing Ni-NTA resin (Qiagen) according to the manufacturer's instructions. The protein was dialyzed against 10 mM Tris−HCl (pH 8.0) and 200 mM NaCl and concentrated to 11.5 mg/mL on the basis of an extinction coefficient of 1.43 $(mg/mL)^{-1}$ cm^{-1}. For removal of the N-terminal His_6 tag, a solution containing a 30:1 molar ratio (WlaRD:TEV protease) was allowed to digest at 4 °C for 48 h. Uncleaved protein and the TEV protease were removed by passage over Ni-NTA resin. Cleaved enzyme was dialyzed and concentrated in the same manner as described above for the N-terminal tagged version.

Synthesis and Purification of the dTDP-Sugar Ligands. dTDP-Qui3N and dTDP-Fuc3N were prepared by modifications of a previously reported procedure.[13] Reactions (15 mL) containing 7 mM dTDP-glucose, 0.4 mg/mL *E. coli* RmlB (a 4,6-dehydratase), 1.9 mg/mL *Thermoanaerobacterium thermosaccharolyticum* QdtA (a 3,4-ketoisomerase), 2.9 mg/mL *T. thermosaccharolyticum* QdtB (an aminotransferase), 40 mM sodium glutamate, and 40 mM HEPPS (pH 8.5) were allowed to react at 37 °C for 12 h to generate dTDP-Qui3N. Substitutions of *Aneurinibacillus thermoaerophilus* FdtA and FdtB for QdtA and QdtB, respectively, were used for the synthesis of dTDP-Fuc3N. Following a 12 h incubation, all enzymes were removed by filtration through a 10 000 MW cutoff Amicon filter. The filtered reaction mixture was then diluted 15-fold with water and loaded onto a 50 mL HiLoad 26/10 Q-Sepharose HP column. The dTDP-amino sugars were purified with a 20-column volume gradient of 0−0.2 M ammonium bicarbonate (pH 8.5) and eluted at a concentration of 0.125 M ammonium bicarbonate. All enzymes required for the syntheses of these sugars were cloned and purified in the laboratory.

N^{10}-formyl-THF was synthesized as previously described.[14] Specifically, N^5-formyl-THF was first converted to 5,10-methylenetetrahydrofolate by mixing 80 mg of N^5-formyl-THF and 160 μL of β-mercaptoethanol in 16 mL of water and adjusting the pH to 1.9 with 0.1 M HCl. The solution was incubated at room temperature for 4 h. The mixture was then converted to N^{10}-formyl-THF by raising the pH to 8.5 with 1 M KOH followed by incubation at 37 °C for 1 h.

For preparation of the dTDP-formylated sugars used in this investigation, 18 mL of the N^{10}-formyl-THF mixture was

dx.doi.org/10.1021/bi4009006 | *Biochemistry* 2013, 52, 6114−6126

combined with 25 mg of dTDP-Qui3N (or dTDP-Fuc3N), 10 mg of WlaRD, and 4 mL of 500 mM HEPPS (pH 8.5) and incubated overnight at 37 °C. The reaction mixture was passed through a 10 000 MW cutoff Amicon filter to remove enzymes, diluted to 500 mL with water, loaded onto a 50 mL HiLoad 26/10 Q-Sepharose HP column, and eluted with a 20-column volume gradient of 0−1.5 M ammonium acetate (pH 4). The dTDP-formylated sugars eluted at a concentration of 600 mM ammonium acetate. The material was diluted, its pH adjusted to 8.5, and the sample loaded onto a second 50 mL 26/10 column for further purification. A 12-column volume gradient of 0−800 mM ammonium bicarbonate (pH 8.5) was used for this step, and the dTDP-formylated sugars eluted at a concentration of 90 mM ammonium bicarbonate. ESI mass spectrometry of the products in negative ion ionization mode gave M-1 peak masses of 574, which corresponded to the calculated masses for the dTDP-formylated sugars.

Crystallization of the WlaRD Complexes. Crystallization conditions were surveyed by the hanging drop method of vapor diffusion using a laboratory-based sparse matrix screen. The enzyme was initially tested in the absence of any added ligands or in the presence of 5 mM dTDP and 5 mM N^5-formyl-THF. The untagged version of the enzyme yielded the best crystals from the initial screens. X-ray diffraction-quality crystals of the protein in complex with dTDP and N^5-formyl-THF were subsequently grown from precipitant solutions composed of 11−15% poly(ethylene glycol) 8000, 200 mM NaCl, and 100 mM MOPS (pH 7). The crystals belonged to the monoclinic space group $C2$ with unit cell dimensions of approximately a = 97.9 Å, b = 63.3 Å, c = 136.2 Å, and β = 110°. The asymmetric unit contained one dimer. Crystals of WlaRD in complex with N^5-formyl-THF and dTDP-Qui3N, dTDP-Fuc3N, or dTDP-Fuc3NFo were prepared in the same manner as described above.

The WlaRD complexes with THF or N^{10}-formyl-THF were generated by first transferring crystals with bound dTDP and N^5-formyl-THF to a synthetic mother liquor composed of 17% poly(ethylene glycol) 8000, 300 mM NaCl, and 100 mM HEPPS (pH 8.5). The mother liquor was exchanged several times in order to remove the bound ligands. The WlaRD/dTDP/N^{10}-formyl-THF complex was then prepared by adding 5 mM dTDP, 7 mM N^{10}-formyl-THF, and 0.3% β-mercaptoethanol to the mother liquor and allowing the crystals to soak for 1 day. The WlaRD/dTDP-glucose/N^{10}-formyl-THF complex was prepared in a similar manner with the substitution of 10 mM dTDP-glucose for dTDP. The dTDP-Qui3N/dTDP-Qui3NFo/THF complex was prepared by soaking the crystals in a solution containing 5 mM dTDP-Qui3N (substrate) and 7 mM N^{10}-formyl-THF (substrate) for 12 h. The enzyme was active in the crystalline lattice such that, in one subunit, dTDP-Qui3N and THF were seen, and in the other subunit, dTDP-Qui3NFo and THF were observed.

Structural Analysis of the WlaRD Complexes. Prior to X-ray data collection at 100 K, all crystals were transferred to a cryo-protectant solution containing 20% poly(ethylene glycol) 8000, 300 mM NaCl, 18% ethylene glycol, and ligands in the same concentrations used for crystallization trials or soaking experiments. X-ray data from the cocrystals were collected at the Structural Biology Center Beamline 19-BM (Advanced Photon Source). The data were processed and scaled with HKL3000.[15] X-ray data from crystals of the complexes generated from the soaking experiments were collected in house using a Bruker AXS Platinum 135 CCD detector controlled with the APEX software

Table 1. X-ray Data Collection Statistics

	dTDP/N^5-formyl-THF	dTDP-Qui3N/ N^5-formyl-THF	dTDP-Fuc3N/ N^5-formyl-THF	dTDP-Fuc3NFo/ N^5-formyl-THF	dTDP/N^{10}-formyl-THF	dTDP-glucose/ N^{10}-formyl-THF	dTDP-Qui3NFo/ dTDP-Qui3N/THF
wavelength (Å)	0.9794	0.9794	0.9794	0.9794	1.5418	1.5418	1.5418
resolution limits (Å)	30.0−1.40 (1.45−1.40)[b]	30.0−1.40 (1.45−1.40)[b]	30.0−1.40 (1.45−1.40)[b]	30.0−1.45 (1.50−1.45)[b]	50.0−1.64 (1.74−1.64)[b]	50.0−1.60 (1.70−1.60)[b]	50.0−1.90 (2.00−1.90)[b]
no. of independent reflections	148 911 (14 019)	143 095 (13 017)	145 264 (12 929)	130 605 (11 745)	93 525 (13 710)	96 212 (13 596)	58 443 (5 762)
completeness (%)	97 (91.7)	92.9 (84.9)	95.5 (84.9)	94.5 (85.5)	96.2 (86.6)	92.8 (79.1)	92.8 (76.5)
redundancy	4.8 (2.9)	3.8 (2.4)	4.1 (2.5)	4.6 (2.8)	4 (1.8)	3.3 (1.4)	3.6 (1.3)
avg I/avg σ (I)	56.7 (18.8)	48.3 (15.5)	48 (9.5)	56.4 (11.5)	14.6 (2.2)	15.6 (2.2)	15.9 (2.3)
R_{sym} (%)[a]	4.6 (7.7)	4.5 (8)	5.5 (12.9)	7.1 (12)	5.8 (36.4)	4.6 (30.5)	5 (26.2)

[a] $R_{sym} = (\sum|I - \bar{I}|/\sum I) \times 100$. [b] Statistics for the highest resolution bin.

dx.doi.org/10.1021/bi4009006 | Biochemistry 2013, 52, 6114−6126

Table 2. Refinement Statistics

	dTDP/ N^5-formyl-THF	dTDP-Qui3N/ N^5-formyl-THF	dTDP-Fuc3N/ N^5-formyl-THF	dTDP-Fuc3NFo/ N^5-formyl-THF	dTDP/N^{10}-formyl-THF	dTDP-glucose/ N^{10}-formyl-THF	dTDP-Qui3NFo/ dTDP-Qui3N/THF
resolution limits (Å)	30−1.4	30−1.4	30−1.4	30−1.45	50−1.64	50−1.6	50−1.9
overall *R* factor[a] (%/no. of reflections)	15.9/148 911	17.9/143 095	18.2/145 264	18.3/130 605	19.1/93 525	17.3/96 212	18.0/58 443
working *R* factor (%/no. of reflections)	15.8/141 466	17.8/135 924	18.0/137 927	18.1/124 054	18.9/88 820	17.1/91 401	17.8/55 503
free *R* factor (%/no. of reflections)	17.8/7445	20.6/7171	21.1/7292	21.2/6551	22.6/4704	20.8/4811	22.6/2940
no. of protein atoms	4645	4633	4631	4625	4555	4570	4483
no. of heteroatoms	1245	1168	1120	975	939	941	771
			Average *B* Values				
protein atoms (Å^2)	13.7	16.0	17.6	17.2	17.3	15.7	18.1
ligand (Å^2)	16.4	14.6	15.6	19.3	31.1	22.5	20.1
solvent (Å^2)	28.6	30.0	32.4	29.9	30.0	27.6	27.8
			Weighted RMS Deviations from Ideality				
bond lengths (Å)	0.012	0.015	0.014	0.012	0.011	0.012	0.013
bond angles (deg)	1.87	2.07	2.14	1.71	2.08	2.24	1.99
planar groups (Å)	0.013	0.009	0.013	0.008	0.011	0.011	0.010
			Ramachandran Regions (%)[b]				
most favored	90.4	91.0	91.0	90.3	89.0	89.9	90.2
additionally allowed	8.8	8.0	8.2	9.2	10.0	9.0	8.5
generously allowed	0.8	1.0	0.8	0.6	1.0	1.2	1.4

[a] *R* factor = $(\Sigma|F_o - F_c|/\Sigma|F_o|) \times 100$, where F_o is the observed structure-factor amplitude and F_c is the calculated structure-factor amplitude. [b] Distribution of Ramachandran angles according to PROCHECK.[24]

Table 3. Kinetic Parameters

substrate	K_m (mM)	k_{cat} (s^{-1})	k_{cat}/K_m (M^{-1} s^{-1})
dTDP-Qui3N	0.110 ± 0.013	1.2 ± 0.1	1.1×10^4
dTDP-Fuc3N	0.630 ± 0.043	0.035 ± 0.004	5.6×10^1

suite (Bruker AXS Inc.) The X-ray source was Cu Kα radiation from a Rigaku RU200 X-ray generator equipped with Montel optics and operated at 50 kV and 90 mA. The data sets were processed with SAINT and scaled with SADABS (Bruker AXS Inc.). Relevant X-ray data collection statistics are listed in Table 1.

The first structure of WlaRD was solved via a three-wavelength MAD experiment using X-ray data collected from the Structural Biology Center Beamline 19-BM. Prior to X-ray data collection, crystals of the WlaRD/dTDP/N^5-formyl-THF complex were soaked for 24 h in a saturated solution of methylmercury acetate and subsequently were prepared for data collection at 100 K as described above. Analysis of the X-ray data with SOLVE located two mercury binding sites.[16] Initial solvent flattened protein phases were calculated with RESOLVE.[17,18] A small region of the protein model was built near the vicinity of each mercury site, which subsequently allowed for the positioning of the local dyad in the asymmetric unit. Molecular averaging and solvent flattening resulted in a greatly improved electron density map that allowed complete tracing of the dimer. The model was then refined against X-ray data collected from the WlaRD/dTDP/N^5-formyl-THF complex crystals. Iterative cycles of model-building with COOT and refinement with REFMAC reduced the R_{work} and R_{free} to 15.8% and 17.8%, respectively, from 30 to 1.4 Å resolution.[19,20] This model was used to solve all of the other structures reported here either by difference Fourier techniques or by molecular replacement with the software package PHASER.[21] Model refinement statistics are listed in Table 2.

Scheme 2

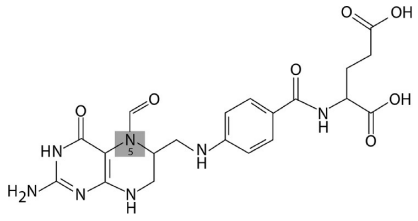

N^5-formyl-THF

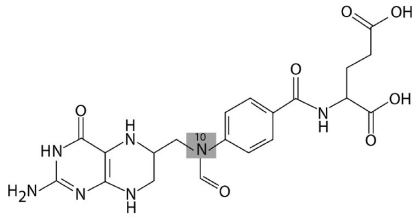

N^{10}-formyl-THF

Kinetic Analyses. Kinetic parameters for WlaRD were determined via a discontinuous assay using an ÄKTA HPLC. The reaction rates were determined by calculating the amount of dTDP-Qui3NFo (or dTDP-Fuc3NFo) produced on the basis of the peak area on the HPLC trace as measured at 267 nm. The area was correlated to concentration via a calibration curve created with standard samples that had been treated in the same manner as the reaction aliquots.

The binding parameters for the dTDP-Qui3N substrate were determined using 1 mL reactions containing 5 mM N^{10}-formyl-THF, 50 mM HEPPS (pH 8.5), 0.03 mg/mL (0.94 μM) enzyme, and substrate concentrations ranging from 0.01 to

dx.doi.org/10.1021/bi4009006 | *Biochemistry* 2013, 52, 6114−6126

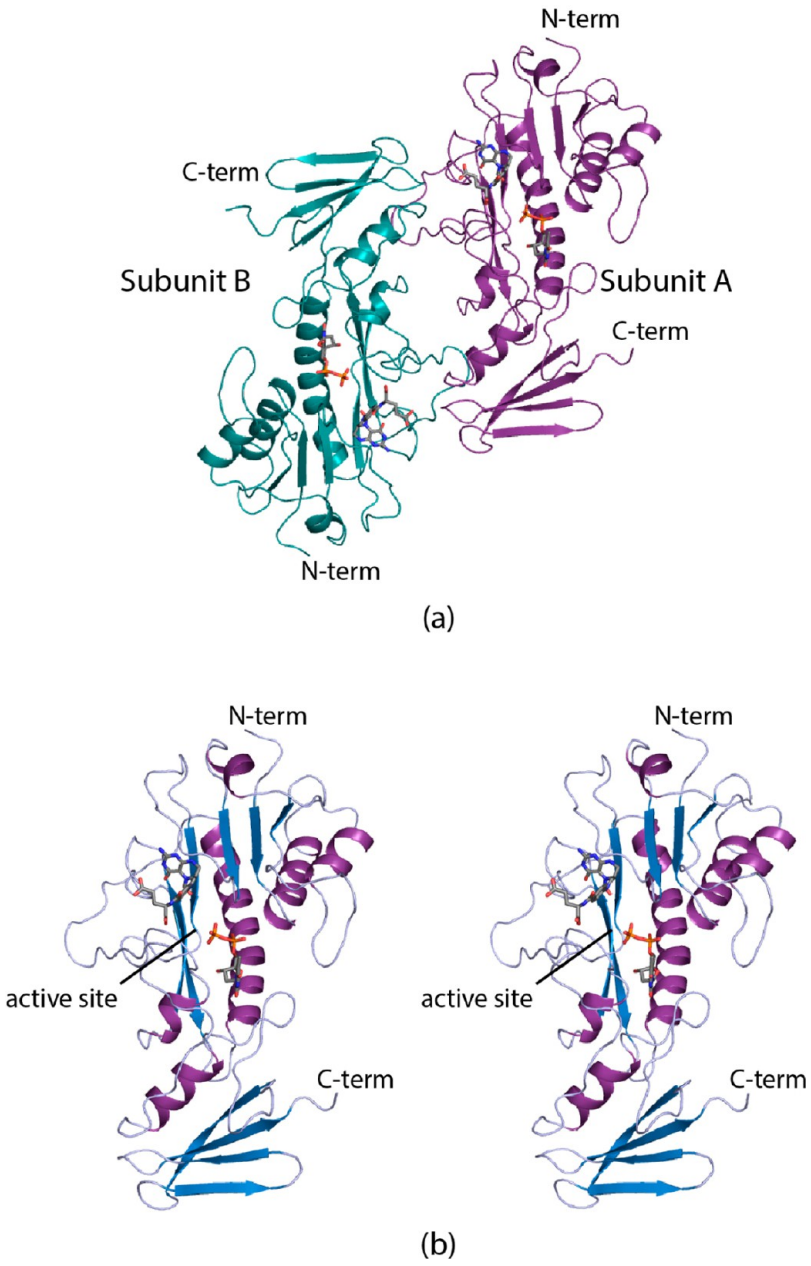

Figure 1. Structure of WlaRD. The first structure of WlaRD was solved in the presence of dTDP and N^5-formyl-THF. (a) Ribbon representation of the WlaRD dimer. The ligands are drawn in stick representation. (b) Stereoview of subunit A. The subunit is distinctly bilobal with the active site wedged between the two domains. All figures were created with PyMOL.[25]

2.0 mM dTDP-Qui3N. Four 250 μL aliquots were taken at time points over 4 min and quenched by the addition of 12 μL of 6 M HCL. Afterward, 200 μL of carbon tetrachloride was added, the samples were vigorously mixed and spun at 14000*g* for 1 min, and 200 μL of the aqueous phase was taken for subsequent analysis via HPLC. The samples were diluted with 2 mL of water and loaded onto a 1 mL ResQ column and the products quantified after elution with an eight-column volume gradient of 0−400 mM LiCl (pH 4, HCl).

The binding parameters for the dTDP-Fuc3N substrate were determined using 1 mL reactions containing 5 mM N^{10}-formyl-THF, 50 mM HEPPS (pH 8.5), 0.15 mg/mL (4.7 μM) enzyme, and substrate concentrations ranging from 0.1 to 6.0 mM dTDP-Fuc3N, and four samples were taken over a 10 min reaction time period for evaluation.

Plots of concentrations versus initial rates were analyzed using PRISM (GraphPad Software, Inc.) and were fitted to the equation $v_o = (V_{max}[S])/(K_M + [S])$. Kinetic parameters are listed in Table 3.

Site-Directed Mutagenesis. The site-directed mutant proteins N94A, H96N, and D132N were generated using the QuikChange method of Stratagene. The protein variants were expressed and purified as described above for the wild-type enzyme. Enzyme activity was assayed at protein concentrations of up to 1 mg/mL (31 μM). Even at the highest concentrations, no measurable quantities of formylated sugars could be detected after reaction times exceeding 4 h.

RESULTS AND DISCUSSION

Overall Structure of the WlaRD/N^5-formyl-THF/dTDP Complex. For the sake of clarity, the chemical structures of

dx.doi.org/10.1021/bi4009006 | *Biochemistry* 2013, 52, 6114−6126

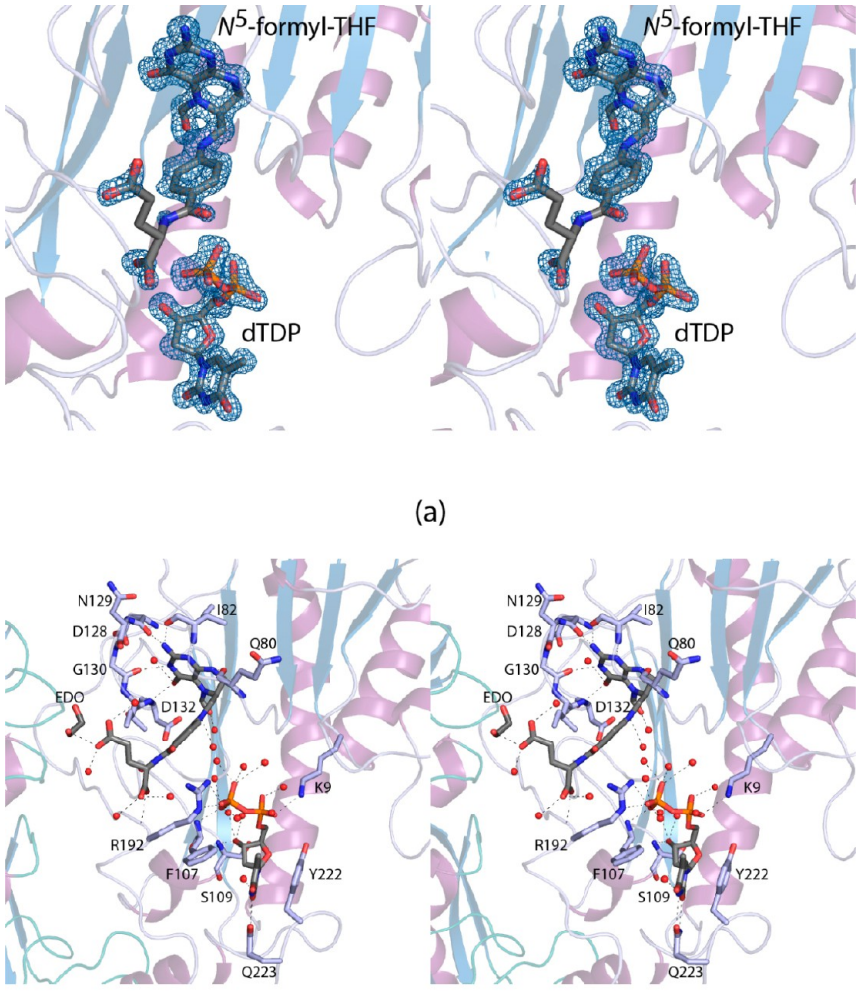

Figure 2. Active site. (a) Electron density corresponding to the bound dTDP and N^5-formyl-THF ligands. The map, contoured at 3σ, was calculated with coefficients of the form $F_o - F_c$ where F_o was the native structure factor amplitude and F_c was the calculated structure factor amplitude. (b) Close-up view of the active site. Water molecules are displayed as red spheres. The dashed lines indicate distances between two atoms of 3.2 Å or less. An ethylene glycol molecule, labeled as EDO, was observed binding in the active site.

N^5-formyl-THF and N^{10}-formyl-THF are provided in Scheme 2. The first structure determined in this investigation was that of the enzyme complexed with N^5-formyl-THF and dTDP. The model was refined to an overall *R* factor of 15.9% at 1.4 Å resolution. A ribbon representation of the WlaRD dimer contained within the asymmetric unit is displayed in Figure 1a. The active sites are separated by over 30 Å. Dimerization results in a total buried surface area of ~2500 Å^2. Subunit A extends from Met 1 to Lys 271, whereas subunit B contains the last C-terminal residue, Leu 272. There are no breaks in the polypeptide chain backbones for either of the subunits. Given that the α-carbons for the two subunits superimpose with a root mean square deviation of 0.19 Å, the following discussion refers only to subunit A unless otherwise indicated.

A stereoview of subunit A is shown in Figure 1b. The overall architecture of the subunit is bilobal with the active site wedged between the two domains. The N-terminal domain, which harbors the binding pocket for the N^5-formyl-THF cofactor, extends from Met 1 to Leu 197 and is dominated by a six-stranded mixed β-sheet flanked on one side by three α-helices and on the other by a small α-helix and random coil. The C-terminal domain, delineated by Val 198 to Lys 271, contains a four-stranded antiparallel β-sheet and an α-helix. Pro 101 adopts a *cis* conformation, but is not involved in the formation of the active site pocket.

Portions of the electron density map corresponding to the bound cofactor and the dTDP ligand are displayed in Figure 2a. As can be seen, the N^5-formyl-THF cofactor adopts a curved conformation with the planes of the 2-amino-4-oxo-6-methylpterin and *p*-aminobenzoic acid moieties tilted at ~90°. A close-up view of the WlaRD active site is presented in Figure 2b. The active site is quite shallow and solvent-accessible. Most of the residues involved in ligand binding are provided by the N-terminal domain. The exceptions are Tyr 222 and Gln 223, which interact with the thymine ring of dTDP via stacking and hydrogen bonding interactions, respectively. Tyr 222 forms a parallel stacking interaction, whereas Phe 107, from the N-terminal domain, participates in a T-shaped interaction. Backbone carbonyl and amide groups are responsible for anchoring the 2-amino-4-oxo-6-methylpterin

dx.doi.org/10.1021/bi4009006 | *Biochemistry* 2013, 52, 6114−6126

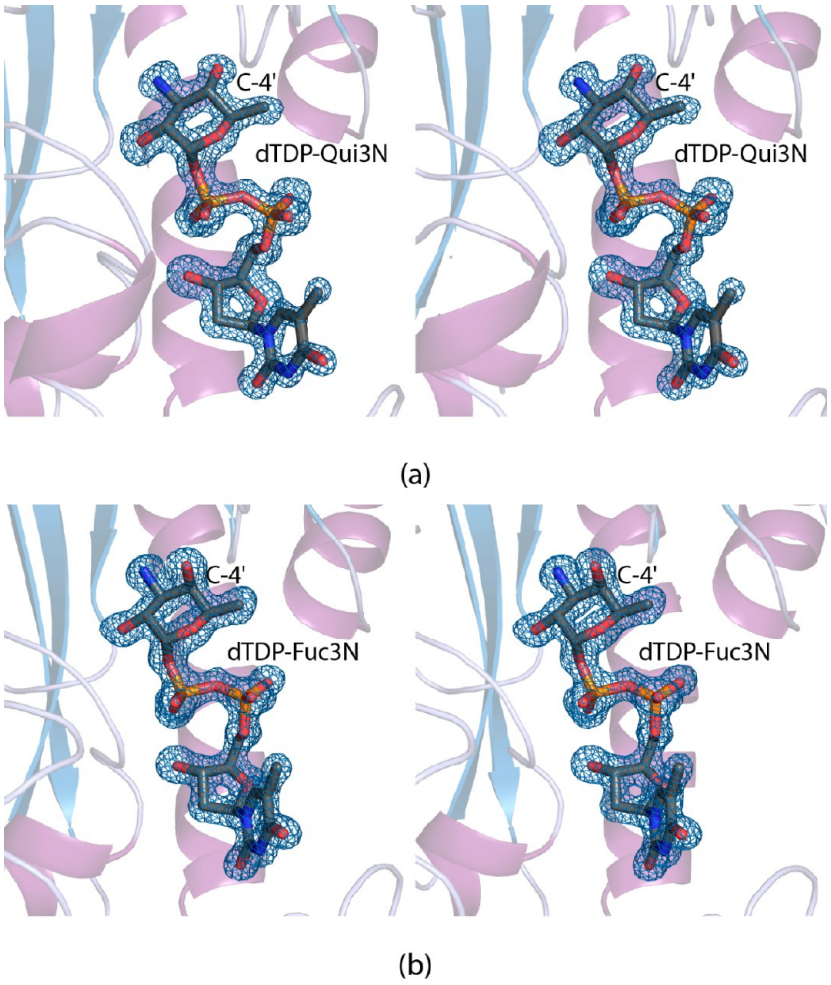

Figure 3. Electron density corresponding to the dTDP-linked sugar substrates. Shown in panels A and B are the electron density maps corresponding to dTDP-Qui3N and dTDP-Fuc3N, respectively. The maps were calculated and contoured as described in the Figure 2 legend.

group of the cofactor into the active site. The formyl group lies within hydrogen bonding distance of a water molecule. There are limited interactions between the protein and the glutamyl moiety of the cofactor, which explains why the electron density is weak in this region. Both Lys 9 and Arg 192 participate in electrostatic interactions with the pyrophosphoryl group of the dTDP ligand.

The WlaRD Active Site with Bound N^5-formyl-THF and Either dTDP-Qui3N or dTDP-Fuc3N. The proposed substrate for WlaRD is dTDP-Qui3N (Scheme 1), although our kinetic analysis shows that the enzyme also functions on dTDP-Fuc3N, albeit at a much reduced rate. Indeed, the catalytic efficiency for dTDP-Fuc3N as a substrate is reduced nearly 200-fold (Table 3). To address the manner in which the enzyme can accommodate two substrates with altered stereochemistries about the hexose C-4′, the structures of both the WlaRD/N^5-formyl-THF/dTDP-Qui3N and the WlaRD/N^5-formyl-THF/dTDP-Fuc3N complexes were solved and refined to 1.4 Å resolution. The observed electron densities corresponding to these bound sugars are presented in Figure 3. Overall, there was little movement in the polypeptide chain backbone upon binding either dTDP-sugar. Indeed, the α-carbons for the WlaRD/N^5-formyl-THF/dTDP model superimpose upon those with bound dTDP-Qui3N or dTDP-Fuc3N with root mean square deviations of 0.20 Å or 0.18 Å, respectively.

Both dTDP-Qui3N and dTDP-Fuc3N anchor into the WlaRD active site via hydrogen bonds with backbone carbonyl groups and ordered water molecules. There are no protein side chains involved in sugar binding. The region of the active site surrounding the C-4′ hydroxyl group is rather open, thus explaining the ability of the enzyme to turn over both substrates. A close-up view of the region near dTDP-Qui3N is shown in Figure 4a, whereas a superposition of the dTDP-sugars in the WlaRD active site is presented in Figure 4b. The pyranosyl moiety of dTDP-Fuc3N is shifted slightly in the active site with respect to that of dTDP-Qui3N such that the amino nitrogen is displaced by 1 Å. This shift in the active site most likely results in the reduced catalytic efficiency of WlaRD toward dTDP-Fuc3N.

A structural alignment between WlaRD, *E. coli* ArnA,[9] *E. coli* L-methionyl-tRNA *N*-formyltransferase,[22] and *E. coli* glycinamide ribonucleotide transformylase[23] reveals three conserved residues located within the active site region: Asn 94, His 96, and Asp 132 (Figure 4a). The N94A, H96N, and D132N site-directed variants showed no enzymatic activity after 4 h of incubation using protein concentrations of up to 1 mg/mL (31 μM).

The WlaRD Active Site with Bound N^5-formyl-THF and dTDP-Fuc3NFo. To explore the manner in which WlaRD binds an *N*-formylated sugar, the next goal in this study was to solve the structure of the enzyme in the presence of N^5-formyl-THF and a formylated product sugar. All attempts to prepare a

dx.doi.org/10.1021/bi4009006 | *Biochemistry* 2013, 52, 6114−6126

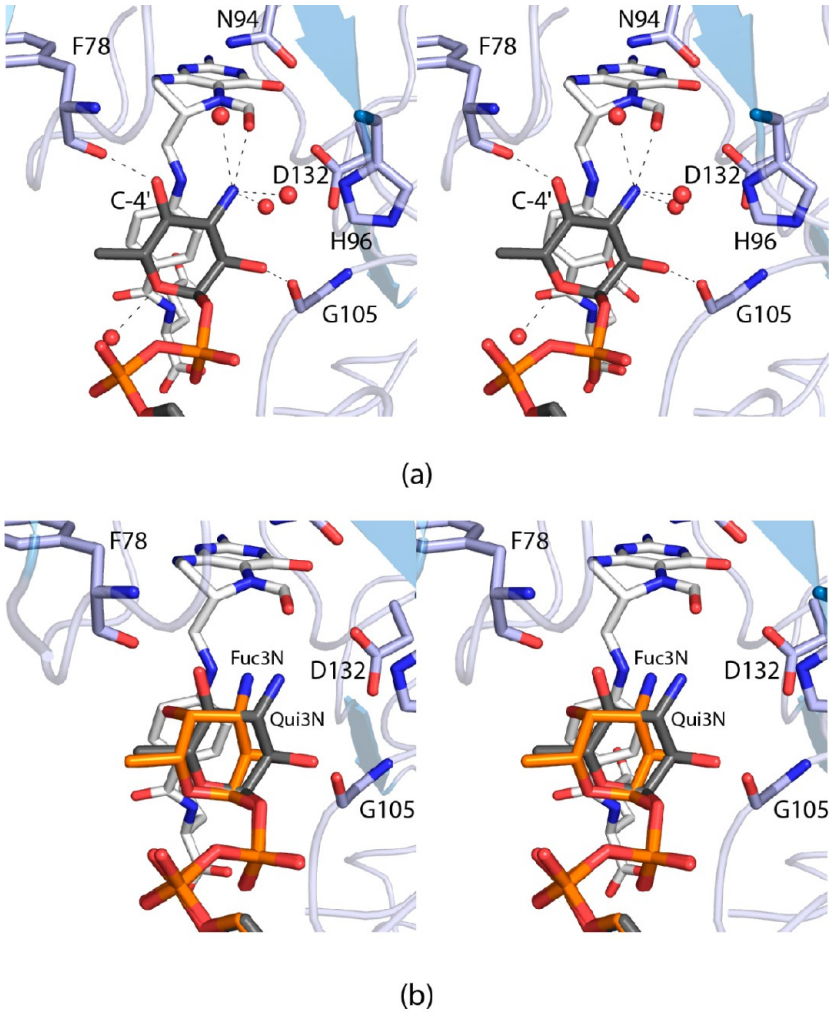

Figure 4. Binding of dTDP-sugars in the WlaRD active site. (a) Close-up view of the active site with bound dTDP-Qui3N. The N^5-formyl-THF cofactor is displayed in white bonds. The dTDP-Qui3N substrate is highlighted in orange and gray bonds. Ordered water molecules lying within 3.2 Å of the hexose moiety are depicted as red spheres. The dashed lines indicate possible hydrogen bonding interactions within 3.2 Å. (b) Superposition of dTDP-Qui3N and dTDP-Fuc3N when bound in the WlaRD active site. dTDP-Qui3N and dTDP-Fuc3N are displayed in gray and orange bonds, respectively.

complex of WlaRD with bound N^5-formyl-THF and dTDP-Qui3NFo were unsuccessful. It was possible, however, to form such a complex in the presence of dTDP-Fuc3NFo as shown in the electron density map presented in Figure 5a. The structure was determined to a nominal resolution of 1.45 Å. There were no major protein conformational changes that occurred upon product binding. The α-carbons for the WlaRD/N^5-formyl-THF/dTDP-Fuc3N and WlaRD/N^5-formyl-THF/dTDP-Fuc3NFo complex models superimpose with a root mean square deviation of 0.10 Å. The only significant changes that occurred were the expulsion of a water molecule from the active site and the movement of the N^5-formyl group of the cofactor (Figure 5b). The *N*-formyl group of the sugar lies within hydrogen bonding distance to Asn 94 and His 96.

The WlaRD Active Site with Bound N^{10}-formyl-THF and Various Ligands. Whereas the first four structures of WlaRD provided an overall view of its molecular architecture and details into its active site, the N^5-formyl-THF cofactor utilized in these investigations is not catalytically competent. For the last three structures determined in this study, crystals previously grown in the presence of dTDP and N^5-formyl-THF were transferred to a synthetic mother liquor lacking these ligands. They were then transferred to solutions containing N^{10}-formyl-THF and dTDP, N^{10}-formyl-THF and dTDP-glucose (substrate analog), or N^{10}-formyl-THF and dTDP-Qui3N (substrate).

The structure of the WlaRD/N^{10}-formyl-THF/dTDP complex was determined to 1.64 Å resolution. The electron density clearly revealed the presence of bound N^{10}-formyl-THF (Figure 6a). The polypeptide chain was virtually unchanged upon binding N^{10}-formyl-THF. Indeed, the α-carbons for the WlaRD/N^{10}-formyl-THF/dTDP and the WlaRD/N^5-formyl-THF/dTDP complexes correspond with a root mean square deviation of 0.21 Å. The major difference occurred around the bridge linking the bicyclic ring to the phenyl moiety of the cofactor. Due to differences in torsional angles, the C-9 carbons of the cofactors are displaced by ~2 Å in the active site cleft (Figure 7a).

The structure of WlaRD in complex with N^{10}-formyl-THF and dTDP-glucose was solved to 1.6 Å resolution. Shown in Figure 6b is the electron density corresponding to these two ligands. Although the density for the dTDP-glucose was well-defined, that corresponding to the phenyl and glutamyl groups of the cofactor was quite weak. This disordering of the phenyl and glutamyl moieties was also observed in the structural

dx.doi.org/10.1021/bi4009006 | *Biochemistry* 2013, 52, 6114−6126

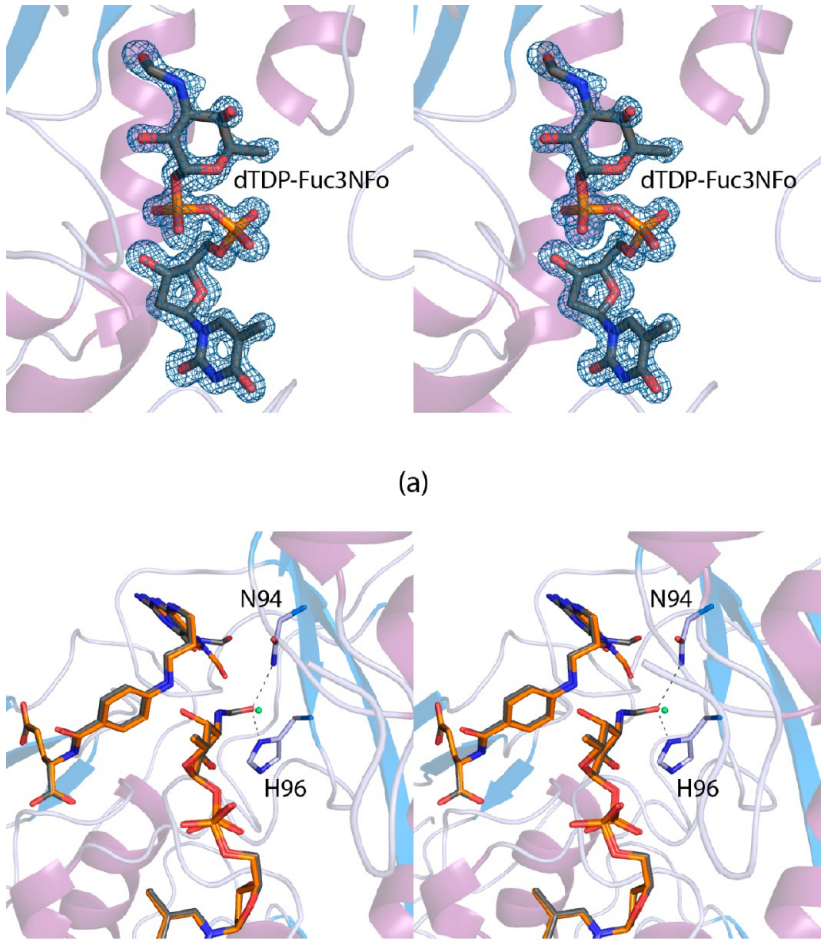

Figure 5. Binding of dTDP-Fuc3NFo in the WlaRD active site. (a) Electron density corresponding to the bound dTDP-sugar. The map was calculated as described in the Figure 2 legend and contoured at 4σ. (b) Comparison on the binding modes for dTDP-Fuc3N (orange bonds) and dTDP-Fuc3NFo (gray bonds). The bound water that moves upon product formation is depicted as a green sphere. The side chains of both Asn 94 and His 96 participate in hydrogen bonding interactions with the oxygen of the *N*-formyl group.

analysis of *E. coli* glycinamide ribonucleotide transformylase.[23] A superposition of the WlaRD active sites with bound N^{10}-formyl-THF and dTDP-glucose versus N^5-formyl-THF and dTDP-Qui3N is displayed in Figure 7b. The α-carbons for the two models superimpose with a root mean square deviation of 0.13 Å. The active site of WlaRD accommodates the presence of the C-6′ hydroxyl group on dTDP-glucose by shifting the hexose moiety out of the binding pocket. As a consequence, its C-3′ hydroxyl group lies at ∼3 Å from where the C-3 amino group of dTDP-Qui3N is located.

For the final structure determined in this investigation, WlaRD crystals were soaked in solutions containing N^{10}-formyl-THF and dTDP-Qui3N with the goal of trapping the reaction products in the active site. In subunit A, THF and dTDP-Qui3N were observed. In subunit B, however, the products THF and dTDP-Qui3NFo were present as indicated by the electron density shown in Figure 6c. Subunits A and B superimpose with a root mean square deviation of 0.19 Å, indicating little conformational change occurred upon binding either dTDP-Qui3N (subunit A) or dTDP-Qui3NFo (subunit B). A close-up view of the WlaRD active site with bound reaction products is displayed in Figure 7c. Four ordered water molecules surround the pyranosyl group of dTDP-Qui3NFo. Strikingly, all three conserved residues, Asn 94, His 96, and Asp 132, lie within 3.2 Å of the *N*-formyl group oxygen. The distance between $O^{\delta 1}$ of Asp 132 and the formyl group oxygen is 2.7 Å, suggesting that the carboxylate group of Asp 132 is protonated following catalysis.

SUMMARY

The first structure of WlaRD, with bound dTDP and N^5-formyl THF, allowed for the molecular architecture of the enzyme to be defined (Figure 1). The next structures with N^5-formyl-THF and either dTDP-Qui3N or dTDP-Fuc3N revealed that the dTDP-Fuc3N ligand shifts in the active site by ∼1 Å relative to dTDP-Qui3N (Figure 4b). This movement is most likely the reason why WlaRD is catalytically less efficient with dTDP-Fuc3N as a substrate. The structure of WlaRD in complex with N^5-formyl-THF and the sugar product, dTDP-Fuc3NFo, showed that both Asn 94 and His 96, which are conserved among the *N*-formyltransferases, sit within hydrogen bonding distance of the oxygen of the sugar *N*-formyl group (Figure 5b).

Of particular importance were the structures of WlaRD solved in the presence of N^{10}-formyl-THF. These models showed, for the first time, the manner in which any *N*-formyltransferase binds N^{10}-formyl-THF. The structure of WlaRD with bound N^{10}-formyl-THF and dTDP demonstrated that there is a

dx.doi.org/10.1021/bi4009006 | *Biochemistry* 2013, 52, 6114−6126

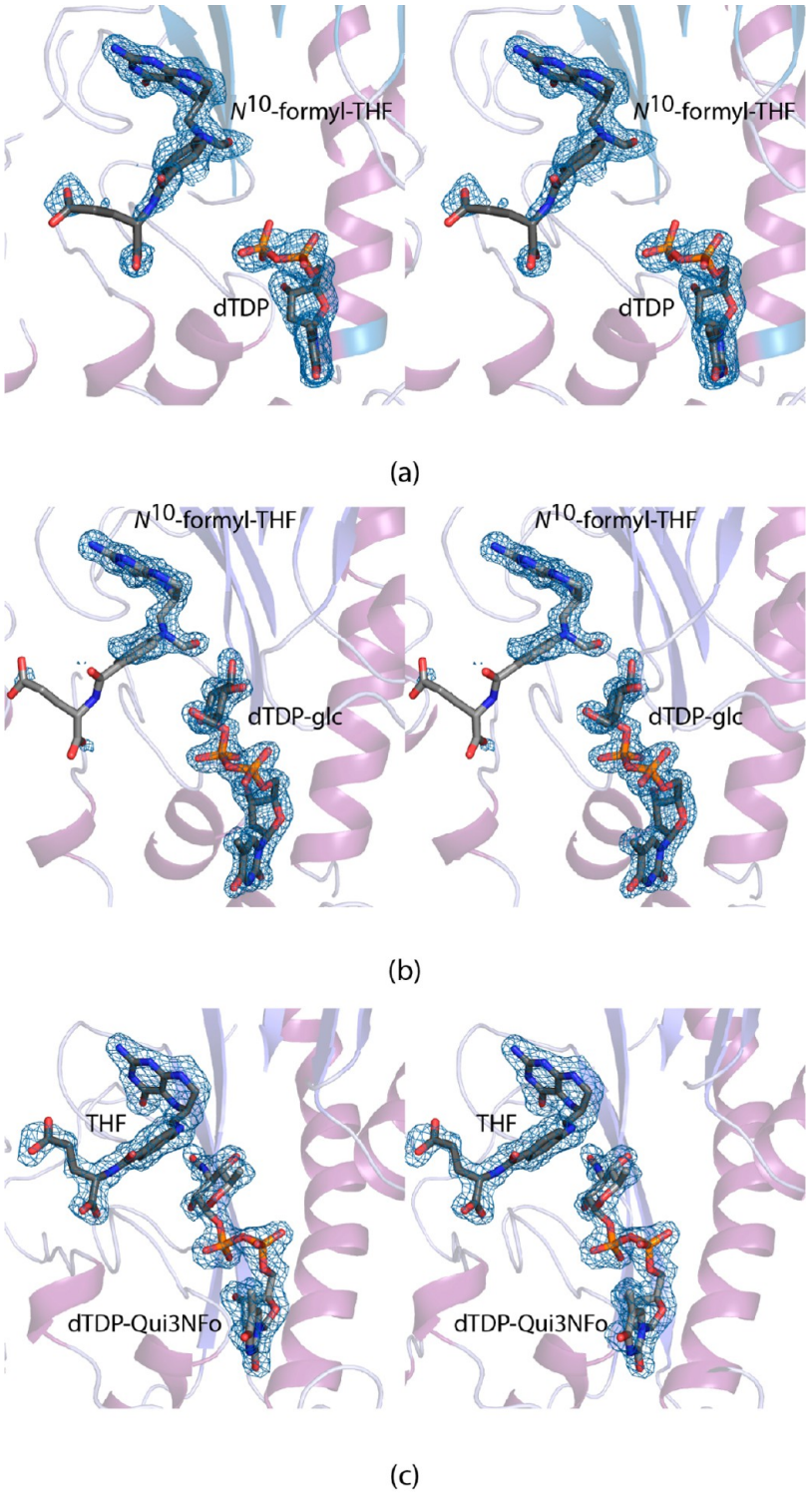

Figure 6. Electron density for the WlaRD/N^{10}-formyl-THF complexes. (a) Electron density corresponding to N^{10}-formyl-THF and dTDP. The map was calculated as described in the Figure 2 legend and contoured at 2.5σ. (b) Electron density corresponding to N^{10}-formyl-THF and dTDP-glucose. The map was contoured at 3σ. (c) Electron density for the products, THF and dTDP-Qui3NFo, bound in subunit B. The map was contoured at 2σ.

difference in rotation about the bridge that links the bicyclic ring to the phenyl moiety of the cofactor (Figure 7a). The structure of WlaRD with bound N^{10}-formyl-THF and dTDP-glucose showed that the WlaRD active site is large enough to accommodate a hydroxyl group at the C′-6 position of a pyranosyl ring, albeit by shifting it out of the active site (Figure 7b).

Clearly the most significant WlaRD structure solved was that with the bound products THF and dTDP-Qui3NFo (Figure 7c). This model represents the active site following catalysis. By superimposing the WlaRD structures in complex with N^{10}-formyl-THF/dTDP and THF/dTDP-Qui3N, it was also possible to generate a model of the active site before catalysis

dx.doi.org/10.1021/bi4009006 | *Biochemistry* 2013, 52, 6114−6126

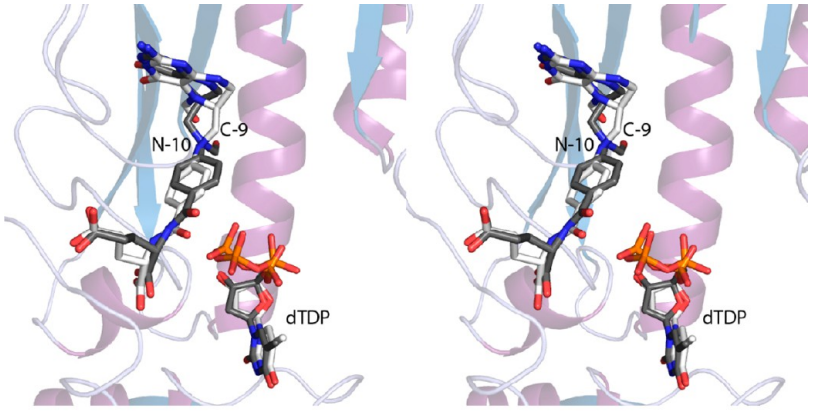

(a)

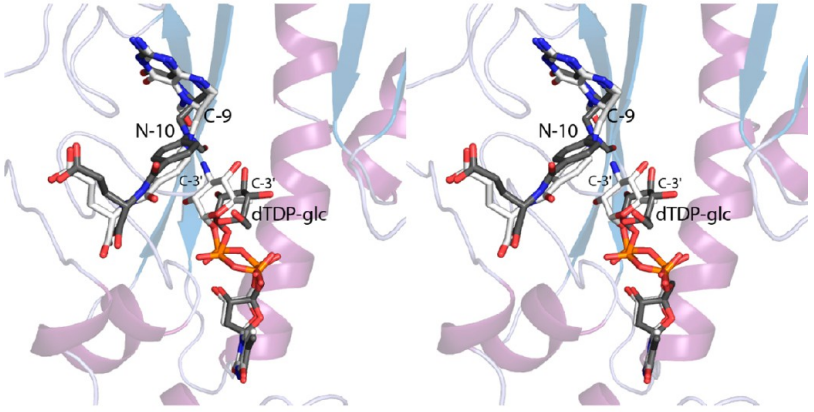

(b)

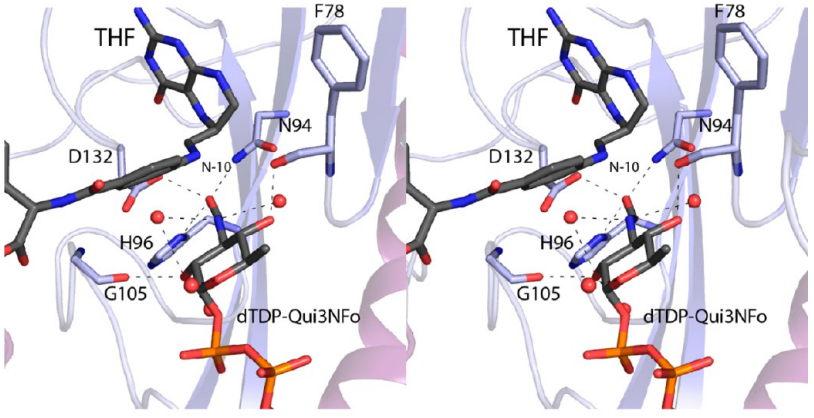

(c)

Figure 7. Close-up views of the WlaRD active site with bound ligands. (a) Differences in binding between N^{10}-formyl-THF, highlighted in gray bonds, and N^{5}-formyl-THF, colored in white bonds, within the WlaRD active site. (b) When dTDP-glucose (gray bonds) binds in the active site, the pyranosyl moiety is shifted from that observed for dTDP-Qui3N (white bonds). (c) WlaRD active site with the bound products THF and dTDP-Qui3NFo. Ordered water molecules are represented by red spheres. Possible hydrogen bonding interactions, within 3.2 Å, are indicated by the dashed lines.

(with N^{10}-formyl-THF and dTDP-Qui3N). Shown in Figure 8 is a superposition of the pre- and postcatalytic states of WlaRD. Upon sugar *N*-formylation, the resulting THF cofactor shifts down in the active site by over 1 Å, whereas the hexose moiety occupies nearly the same position. The amino nitrogen of the substrate lies approximately on the *re* face of the formyl group on N^{10}-formyl-THF. For glycinamide ribonucleotide transformylase, it has been proposed that the conserved histidine accepts a

dx.doi.org/10.1021/bi4009006 | *Biochemistry* 2013, 52, 6114−6126

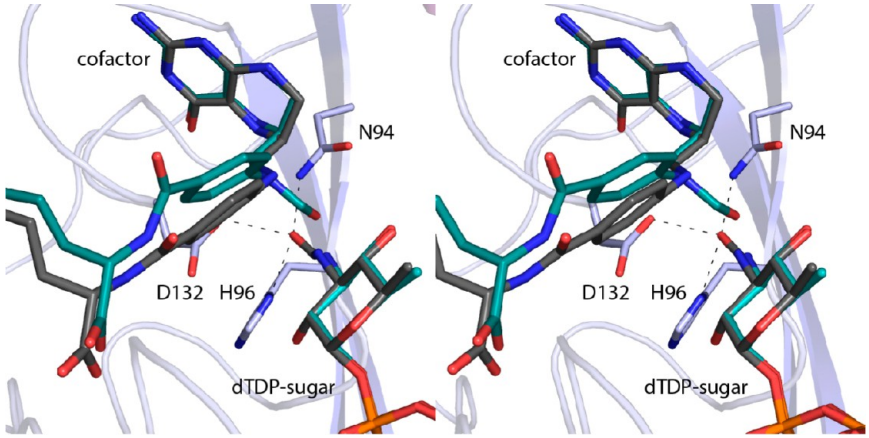

Figure 8. WlaRD active site before and after catalysis. A superposition of the binding positions for N^{10}-formyl-THF and dTDP-Qui3N (in teal) and THF and dTDP-Qui3NFo (in gray) is shown. The three residues that are conserved among *N*-formyltransferases, Asn 94, His 96, and Asp132, are all located within hydrogen bonding distance of the oxygen of the *N*-formyl group on the sugar (dashed lines).

proton from the substrate's amino group as it attacks the formyl carbon of the cofactor, resulting in a tetrahedral transition state.[23] Although both His 96 and Asp 132 in WlaRD could possibly function in such a role, the imidazole ring of His 96 appears to be in a more suitable orientation for proton abstraction (Figure 8). The fact that Asp 132 is within hydrogen bonding distance of the formyl oxygen of the sugar product suggests that it is protonated after catalysis. Its protonation state before catalysis is unknown. Importantly, mutation of either His 96 or Asp 132 resulted in an inactive protein under the assay conditions employed. When Asn 94 was mutated to an alanine, all activity was lost. As suggested for glycinamide ribonucleotide transformylase, it is possible that this conserved asparagine residue plays a role in the formation of an oxyanion hole required to stabilize the negatively charged oxygen of the tetrahedral transition state.

In conclusion, the series of high-resolution structural analyses presented here has provided a detailed description of the molecular architecture of WlaRD and serves as a paradigm for bacterial *N*-formyltransferases that function on nucleotide-linked sugars.

■ ASSOCIATED CONTENT

Accession Codes

X-ray coordinates have been deposited in the Research Collaboratory for Structural Bioinformatics, Rutgers University, New Brunswick, N. J. (accession nos. 4LXQ, 4LXT, 4LXU, 4LXX, 4LXY, 4LY0, and 4LY3).

■ AUTHOR INFORMATION

Corresponding Author

*E-mail: Hazel_Holden@biochem.wisc.edu. Fax: 608-262-1319. Phone: 608-262-4988.

Funding

¶This research was supported in part by an NIH grant (DK47814 to H.M.H.).

Notes

The authors declare no competing financial interest.

■ ACKNOWLEDGMENTS

We thank Professor Grover Waldrop for helpful comments. A portion of the research described in this paper was performed at Argonne National Laboratory, Structural Biology Center at the Advanced Photon Source (U.S. Department of Energy, Office of Biological and Environmental Research, under Contract DE-AC02-06CH11357). We gratefully acknowledge Dr. Norma E. C. Duke for assistance during the X-ray data collection at Argonne.

Abbreviations:; dTDP, thymidine diphosphate; dTDP-Fuc3N, dTDP-3-amino-3,6-dideoxy-D-galactose; dTDP-Fuc3NFo, dTDP-3,6-dideoxy-3-formamido-D-galactose; dTDP-Qui3N, dTDP-3-amino-3,6-dideoxy-D-glucose; dTDP-Qui3NFo, dTDP-3,6-dideoxy-3-formamido-D-glucose; ESI, electrospray ionization; HEPPS, *N*-2-hydroxyethylpiperazine-*N*′-3-propanesulfonic acid; HPLC, high-performance liquid chromatography; IPTG, isopropyl β-D-1-thiogalactopyranoside; MOPS, 3-(*N*-morpholino)-propanesulfonic acid; N^5-formyl-THF, N^5-formyltetrahydrofolate N^{10}-formyl-THF N^{10}-formyltetrahydrofolate; Ni-NTA, Ni nitrilotriacetic acid; NMR, nuclear magnetic resonance; PCR, polymerase chain reaction; TEV, tobacco etch virus; THF, tetrahydrofolate; Tris, *tris*-(hydroxymethyl)-aminomethane

■ REFERENCES

(1) Moran, A. P., Prendergast, M. M., and Appelmelk, B. J. (1996) Molecular mimicry of host structures by bacterial lipopolysaccharides and its contribution to disease. *FEMS Immunol. Med. Microbiol. 16*, 105−115.

(2) Raetz, C. R., and Whitfield, C. (2002) Lipopolysaccharide endotoxins. *Annu. Rev. Biochem. 71*, 635−700.

(3) Thibodeaux, C. J., Melancon, C. E., III, and Liu, H. W. (2008) Natural-product sugar biosynthesis and enzymatic glycodiversification. *Angew. Chem., Int. Ed. Engl. 47*, 9814−9859.

(4) Skurnik, M., and Bengoechea, J. A. (2003) The biosynthesis and biological role of lipopolysaccharide O-antigens of pathogenic *Yersiniae*. *Carbohydr. Res. 338*, 2521−2529.

(5) Lin, C. I., McCarty, R. M., and Liu, H. W. (2013) The biosynthesis of nitrogen-, sulfur-, and high-carbon chain-containing sugars. *Chem. Soc. Rev. 42*, 4377−4407.

(6) Knirel, Y. A., Vinogradov, E. V., Shashkov, A. S., Dmitriev, B. A., Kochetkov, N. K., Stanislavsky, E. S., and Mashilova, G. M. (1985) Somatic antigens of *Pseudomonas aeruginosa*. The structure of the O-specific polysaccharide chains of lipopolysaccharides of *P. aeruginosa* serogroup O4 (Lanyi) and related serotype O6 (Habs) and immunotype 1 (Fisher). *Eur. J. Biochem. 150*, 541−550.

(7) Breazeale, S. D., Ribeiro, A. A., McClerren, A. L., and Raetz, C. R. (2005) A formyltransferase required for polymyxin resistance in *Escherichia coli* and the modification of lipid A with 4-amino-4-deoxy-L-arabinose. Identification and function of UDP-4-deoxy-4-formamido-L-arabinose. *J. Biol. Chem. 280*, 14154−14167.

(8) Liu, B., Chen, M., Perepelov, A. V., Liu, J., Ovchinnikova, O. G., Zhou, D., Feng, L., Rozalski, A., Knirel, Y. A., and Wang, L. (2012) Genetic analysis of the O-antigen of *Providencia alcalifaciens* O30 and biochemical characterization of a formyltransferase involved in the synthesis of a Qui4N derivative. *Glycobiology 22*, 1236−1244.
(9) Williams, G. J., Breazeale, S. D., Raetz, C. R., and Naismith, J. H. (2005) Structure and function of both domains of ArnA, a dual function decarboxylase and a formyltransferase, involved in 4-amino-4-deoxy-L-arabinose biosynthesis. *J. Biol. Chem. 280*, 23000−23008.
(10) Holden, K. M., Gilbert, M., Coloe, P. J., Li, J., and Fry, B. N. (2012) The role of WlaRG, WlaTB and WlaTC in lipooligosaccharide synthesis by *Campylobacter jejuni* strain 81116. *Microb. Pathog. 52*, 344−352.
(11) Muldoon, J., Shashkov, A. S., Moran, A. P., Ferris, J. A., Senchenkova, S. N., and Savage, A. V. (2002) Structures of two polysaccharides of *Campylobacter jejuni* 81116. *Carbohydr. Res. 337*, 2223−2229.
(12) Thoden, J. B., and Holden, H. M. (2005) The molecular architecture of human *N*-acetylgalactosamine kinase. *J. Biol. Chem. 280*, 32784−32791.
(13) Thoden, J. B., Cook, P. D., Schaffer, C., Messner, P., and Holden, H. M. (2009) Structural and functional studies of QdtC: an *N*-acetyltransferase required for the biosynthesis of dTDP-3-acetamido-3,6-dideoxy-alpha-D-glucose. *Biochemistry 48*, 2699−2709.
(14) Breazeale, S. D., Ribeiro, A. A., and Raetz, C. R. (2002) Oxidative decarboxylation of UDP-glucuronic acid in extracts of polymyxin-resistant *Escherichia coli*. Origin of lipid a species modified with 4-amino-4-deoxy-L-arabinose. *J. Biol. Chem. 277*, 2886−2896.
(15) Minor, W., Cymborowski, M., Otwinowski, Z., and Chruszcz, M. (2006) HKL-3000: the integration of data reduction and structure solution-from diffraction images to an initial model in minutes. *Acta Crystallogr., Sect. D: Biol. Crystallogr. 62*, 859−866.
(16) Terwilliger, T. C., and Berendzen, J. (1999) Automated MAD and MIR structure solution. *Acta Crystallogr., Sect. D: Biol. Crystallogr. 55* (Pt 4), 849−861.
(17) Terwilliger, T. C. (2000) Maximum-likelihood density modification. *Acta Crystallogr., Sect. D: Biol. Crystallogr. 56* (8), 965−972.
(18) Terwilliger, T. C. (2003) Automated main-chain model building by template matching and iterative fragment extension. *Acta Crystallogr., Sect. D: Biol. Crystallogr. 59*, 38−44.
(19) Murshudov, G. N., Vagin, A. A., and Dodson, E. J. (1997) Refinement of macromolecular structures by the maximum-likelihood method. *Acta Crystallogr., Sect. D: Biol. Crystallogr. 53*, 240−255.
(20) Emsley, P., and Cowtan, K. (2004) Coot: model-building tools for molecular graphics. *Acta Crystallogr., Sect. D: Biol. Crystallogr. 60*, 2126−2132.
(21) McCoy, A. J., Grosse-Kunstleve, R. W., Adams, P. D., Winn, M. D., Storoni, L. C., and Read, R. J. (2007) Phaser crystallographic software. *J. Appl. Crystallogr. 40*, 658−674.
(22) Schmitt, E., Blanquet, S., and Mechulam, Y. (1996) Structure of crystalline *Escherichia coli* methionyl-tRNA(f)Met formyltransferase: comparison with glycinamide ribonucleotide formyltransferase. *EMBO J. 15*, 4749−4758.
(23) Almassy, R. J., Janson, C. A., Kan, C. C., and Hostomska, Z. (1992) Structures of apo and complexed *Escherichia coli* glycinamide ribonucleotide transformylase. *Proc. Natl. Acad. Sci. U. S. A. 89*, 6114−6118.
(24) Laskowski, R. A., Moss, D. S., and Thornton, J. M. (1993) Main-chain bond lengths and bond angles in protein structures. *J. Mol. Biol. 231*, 1049−1067.
(25) DeLano, W. L. (2002) *The PyMOL Molecular Graphics System*. DeLano Scientific, San Carlos, CA.